SAND2017-8300R

ART End User Applications
Task 2.04.19.06
Supercritical Transformational Electric Power (STEP)

Milestone Report

Resolving Turbine Degradation

Alan Kruizenga, Matthew Walker, Elizabeth Withey

Sandia National Laboratories

August 2, 2017

S-CO2 Materials Development
Work Package: AT-17SN190602 (STEP – 2)
Level 3 Milestone Report: M3AT-17SN1906024

ABSTRACT

The supercritical carbon dioxide (S-CO2) Brayton Cycle has gained significant attention in the last decade as an advanced power cycle capable of achieving high efficiency power conversion. Sandia National Laboratories, with support from the U.S. Department of Energy Office of Nuclear Energy (US DOE-NE), has been conducting research and development in order to deliver a technology that is ready for commercialization.

Root cause analysis has been performed on the Recompression Loop at Sandia National Laboratories. It was found that particles throughout the loop are stainless steel, likely alloy 316 based upon the elemental composition. Deployment of a filter scheme is underway to both protect the turbomachinery and also for purposes of determining the specific cause for the particulate.

Shake down tests of electric resistance (ER) as a potential in-situ monitoring scheme shows promise in high temperature systems. A modified instrument was purchased and held at 650°C for more than 1.5 months to date without issue. Quantitative measurements of this instrument will be benchmarked against witness samples in the future, but all qualitative trends to date are as to be expected. ER is a robust method for corrosion monitoring, but very slow at responding and can take several weeks under conditions to see obvious changes in behavior. Electrochemical noise was identified as an advanced technique that should be pursued for the ability to identify transients that would lead to poor material performance.

NOMENCLATURE

$S\text{-}CO_2$ = Supercritical Carbon Dioxide
US DOE-NE = United States Department of Energy – Nuclear Energy Division
ER = Electrical Resistance
NE = Nuclear Energy
DOE = Department of Energy
sCO2 = Supercritical Carbon Dioxide
SFR = Sodium Fast Reactor
RCBC = Recompression Closed Brayton Cycle
PCHE = Printed Circuit Heat Exchanger
TAC = Turbine-Alternator-Compressor
RCA = Root Cause Analysis
OUO = Official Use Only
SEM = Scanning Electron Microscope
EDS = Energy Dispersive Spectroscopy
FMA = Failure Mode Assessment
TPR = Technical Plan of Resolution
XRD = X-ray Diffraction
PTL = Particle Technology Lab
AR = Aspect Ratio
CBC = Closed Brayton Cycle

CONTENTS

FIGURES

TABLES

1. Introduction

Advanced power cycle conversion continues to be an important area of global research as ever increasing demands for electricity require greater conversion efficiency, while keeping the levelized cost of electricity low. Office of Nuclear Energy (NE) at the Department of Energy (DOE) has identified the supercritical carbon dioxide (sCO_2) Brayton cycle as a candidate energy conversion cycle for the Sodium Fast Reactor (SFR) concept that is currently being evaluated for next generation reactor feasibility.

The NE energy conversion program has both modeling and experimental aspects meant to reduce risk and inform the nuclear power community as a whole as to the workings of sCO_2 technology. Experimental sCO_2 is primarily located at Sandia National Laboratories (located in Albuquerque New Mexico) which consists of a Recompression Closed Brayton Cycle (RCBC) that is illustrated schematically in Figure 1, consisting of several Printed Circuit Heat Exchangers (PCHEs), two turbine-alternator-compressors (TACs), a primary heater, system piping, and instrumentation. Over the last several years degradation has occurred in several forms, both in some fouling of the recuperators and in excessive wear of the turbomachinery (SAND2014-16991C).

Fouling of the heat exchangers was due to insufficient cleaning of the piping material and was rectified by change in the cleaning procedure upon reception of system piping and has not been observed since. Turbomachinery wear has persisted since the original work performed in 2014, thus a more complete root cause analysis (RCA) was undertaken in 2016 to better understand the possible underlying causes of wear and if remedial action could mitigate further wear.

Overall goals of this process were to not only identify improvements in design and operation, but also to find gaps in knowledge and information. Gaps would be alleviated by inclusion of new maintenance schedules, sensor technology, or operation practices that would increase component reliability and lifetimes.

1. RCA Meeting and Failure Modes Analysis (February 2016)
2. Initial RCBC Root Cause Analysis Inspection (July 2016)
3. Primary Heater Inspection (January 2017)
4. Preliminary Conclusions and Associated Actions (March 2017)
5. Corrosion Sensor Development (July 2017)

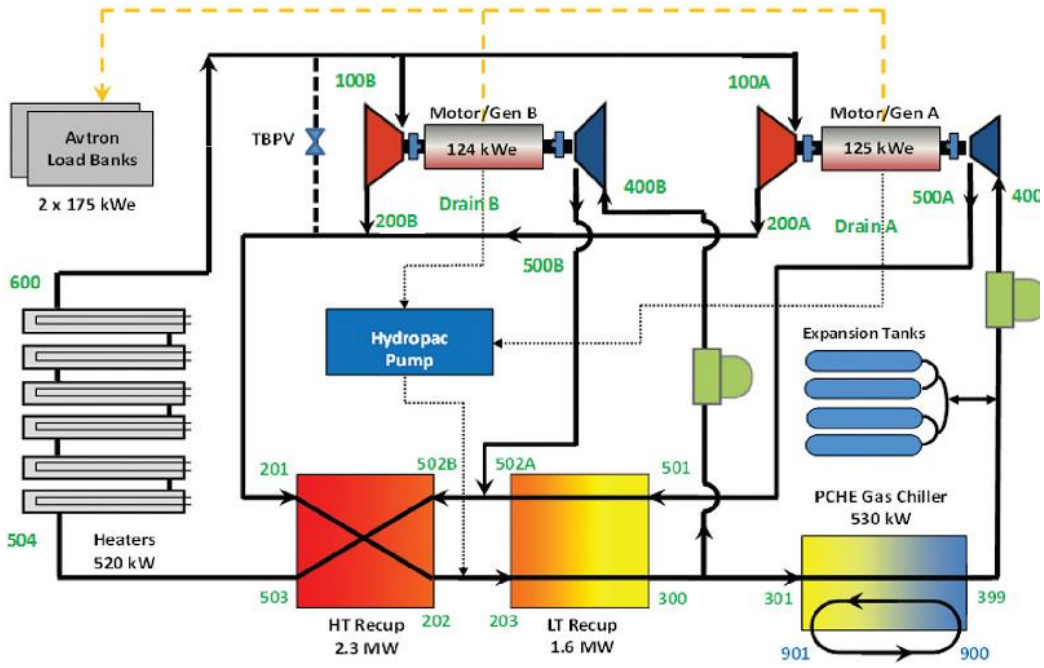

Figure 1: RCBC schematic

2. RCA Investigation to Resolve Turbine Degradation

2.1. Background

The bulk of this section was taken directly from a previous milestone report (M3ST-16SN0101053) [1]. Since this document contained Official Use Only (OUO) information, it was necessary to remove the relevant data for open dissemination.

A consistent observation in the operation of Sandia's sCO_2 RCBC test loop has been turbine degradation. This has only been observed for the turbine and not for the compressor. Also, while it has been observed both for the turbine wheel and turbine nozzle, it has been primarily observed as wear of the turbine nozzle. The alloy in both instances is Alloy 718.

Focusing on the turbine nozzle, two forms of degradation have been observed. One form, shown in Figure 2, is the pitting of nozzle surfaces resulting in a matte surface finish that resembles that of a grit-blasted surface. The other form, shown in Figure 3, involves the thinning and eventual deformation of the thinnest sections of the nozzle.

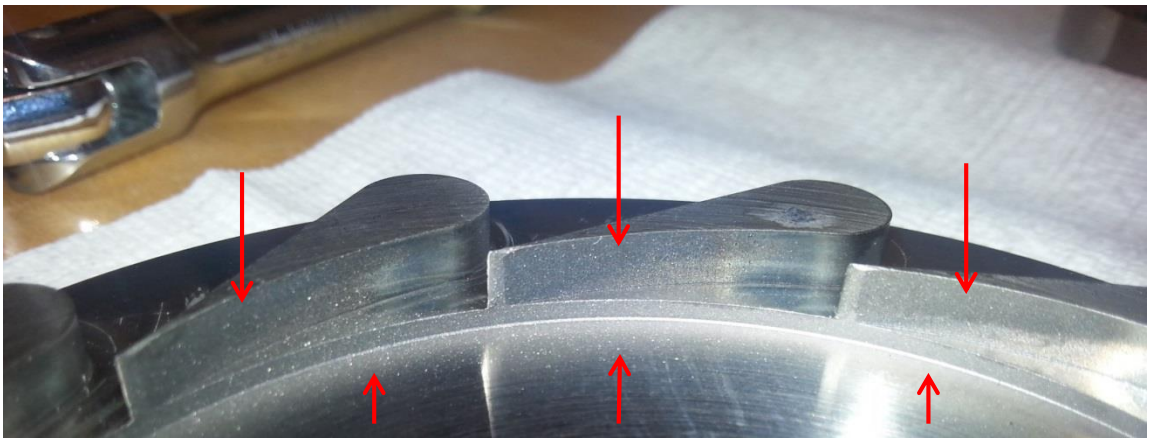

Figure 2: Turbine nozzle showing areas of metal pitting/wear (indicated by arrows).

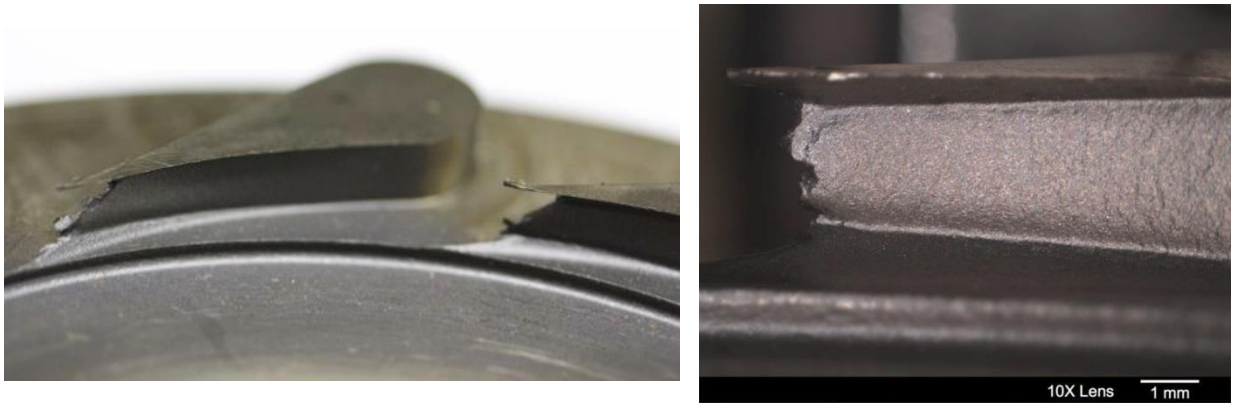

Figure 3: Excessive pitting and wear observed for flow directing portion of a turbine nozzle.

Some analyses have been conducted by Sandia in the past to understand this issue. Although these did not identify the specific cause for the observed degradation, they did provide some valuable information.

First, an analysis of the operational regime during normal operation within the turbine indicated that liquid impingement should never be an issue with sCO_2, and that all wear should be attributed to non-liquid erosion. Liquid impingement during start up is unlikely due to use of a turbine by-pass valve until CO_2 temperatures are above 100°C ensuring that the fluid is in the gas-like regime at all times.

Microscopic characterization of worn vs. non-worn surfaces indicated significant differences both in terms of appearance and chemistry. In Figure 4, scanning electron microscopy (SEM) images of two separate surfaces are shown at two magnifications. In the case of Surface 2, this is a non-flow surface and one that did not show visible wear. Microscopically, this surface appears rather smooth and unchanged during operation in the test loop; machining marks from when the part was made are evident. Chemical analyses of this surface using Energy Dispersive Spectroscopy (EDS) revealed little change to the surface chemistry compared to that of the original alloy. Conversely, Surface 3 is the path of flow and one that had visible wear evident by its characteristic matte finish. Now, no machining artifacts were present on the surface; instead, the surface showed increased roughness resembling wear damage. Also, the surface chemistry showed significant iron enrichment as compared to the original alloy.

Based on this information, the cause for the observed wear was believed to be due to impingement of iron-rich particles with surfaces in the gas flow path. Furthermore, a hypothesis was developed that the source of these particles was the spallation of iron oxide from the interior walls of carbon steel gas inventory tanks; prior to use in the test loop, hydro pressure testing may have caused internal oxidation within the tanks. Testing was never conducted to prove this hypothesis. As a result, the specific cause of observed turbine degradation was unclear.

This presented significant risk to future development of this process, if not completely understood and resolved at the smaller scale of the current test system. In order to fully understand and resolve this issue, a detailed failure investigation has been performed. A key element of this is conducting a root cause analysis (RCA) for turbine degradation.

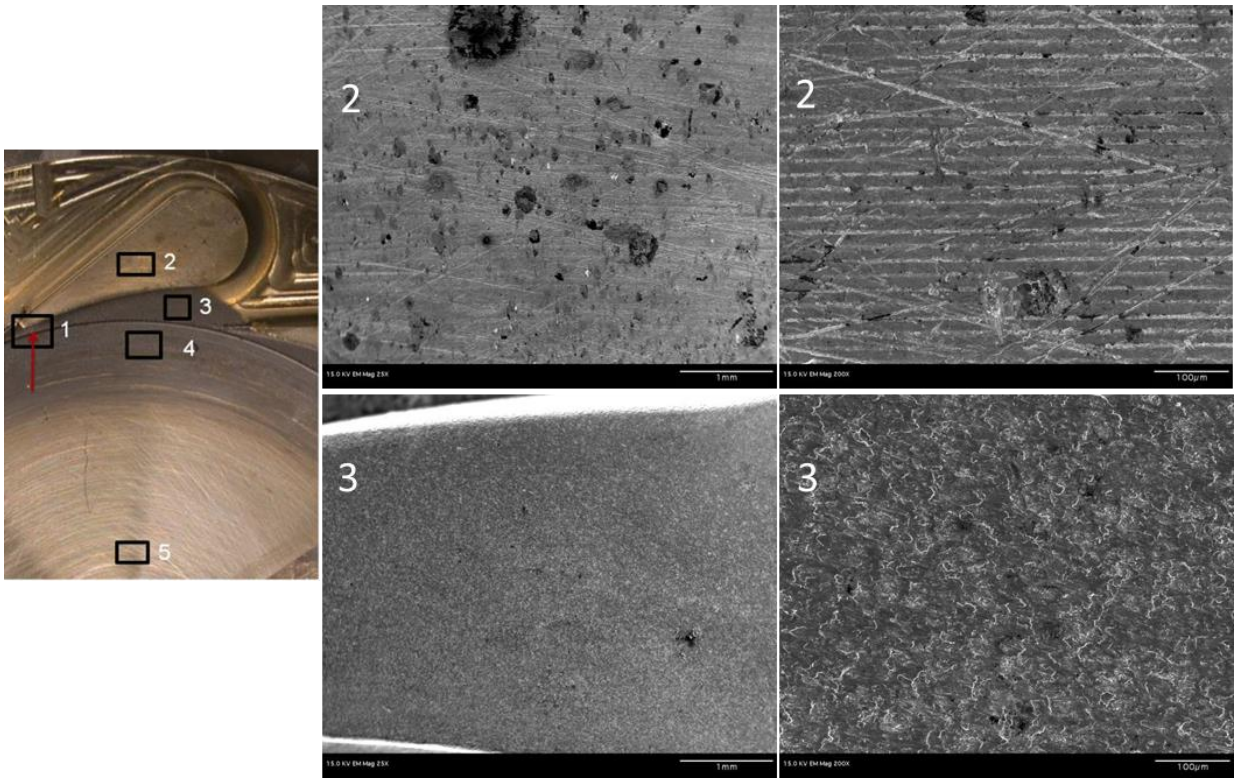

Figure 4: Comparison of a non-flow surface with no wear (2) to a surface in the flow path with evident wear (3).

2.2. RCA Approach

The specific process used to conduct this failure investigation was prepared using a valuable resource from ASM International and Daniel P. Dennies, *How to Organize and Run a Failure Investigation*[2]. In this book, the author describes a plan for finding the root cause of a particular failure, and to ultimately implement effective corrective actions to eliminate it. Here, the process is applied to resolving an identified problem, turbine degradation, as opposed to an outright failure.

The major steps in this process are shown in Figure 5. A team of Sandia contributors across a range of expertise were identified to participate in each step of the process. The first step was to complete an RCA. This is focused on first obtaining a clear understanding of the failure, followed by identification of all possible root causes in the form of a fault tree. Converging on the most likely root cause is the focus of the next two steps. This is done by prioritizing and evaluating the identified root causes in the fault tree. The final three steps involve the identification and implementation of an optimal corrective action to eliminate turbine degradation.

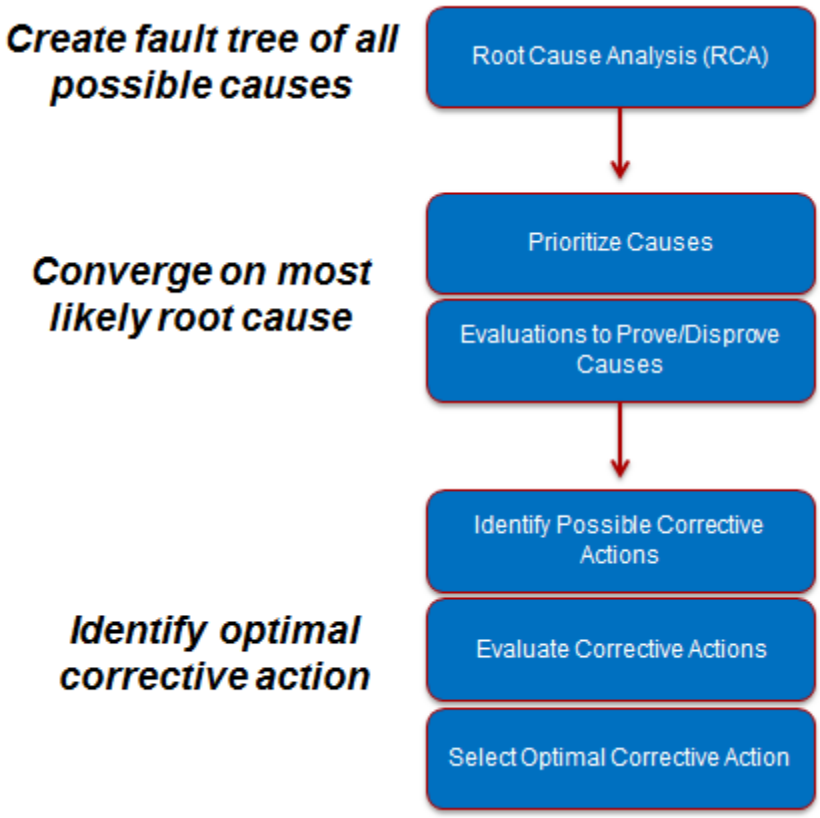

Figure 5: Failure investigation process flow diagram.

2.3. RCA Preliminary Assessment

In February 2016 a team of seven contributors gathered in Albuquerque, New Mexico for two days to complete the first step in the failure investigation process. During the first day, information was presented describing the current state of knowledge regarding turbine degradation. A brainstorming activity during the second day resulted in the creation of a detailed fault tree containing over 60 possible causes across 5 main categories. These categories include Foreign Materials, Turbine Materials, Turbine Design, Process Operations, and Turbine-Alternator-Compressor (TAC) Build; each of the categories along with their identified causes are shown in Figure 6 through Figure 10, respectively.

The 60 possible causes in the fault tree are far too many to evaluate in depth. During a subsequent teleconference, the team reconvened to prioritize each of the identified causes using a Failure Mode Assessment (FMA). Here, each of the causes was discussed, ultimately assigning a probability to it along with the rationale for doing so. This resulted in a list of 11 high priority causes across each of the 5 main categories. These are listed in Table 1 as part of a detailed Technical Plan of Resolution (TPR) for evaluating each of the priority causes.

The TPR includes plans for evaluating each of the high priority causes, along with the individuals responsible for completing each evaluation. Of these 11 possible causes, plans were established to evaluate 9 of them. The remaining two causes, focused around the TAC Build, are viewed as lower

priority, and will be evaluated only if the other causes are found to be disproven. The plans for the other nine causes involve a mixture of experimental and non-experimental evaluations. Experimental evaluations, mainly focused on identifying sources for particles within the loop, will utilize a combination of particulate filters along with borescope inspection cameras (see next section).

Areas to investigate include CO_2 bottles, inventory/expansion tanks, heaters, loop interior piping and ports (burrs), and bearing surfaces. Non-experimental evaluations are focused on the turbine materials and turbine design. In both instances, the emphasis is on working with others (turbine vendor and turbine design shop) to ensure that the materials and design are appropriate for the application, and are not contributing to the degradation that has been observed.

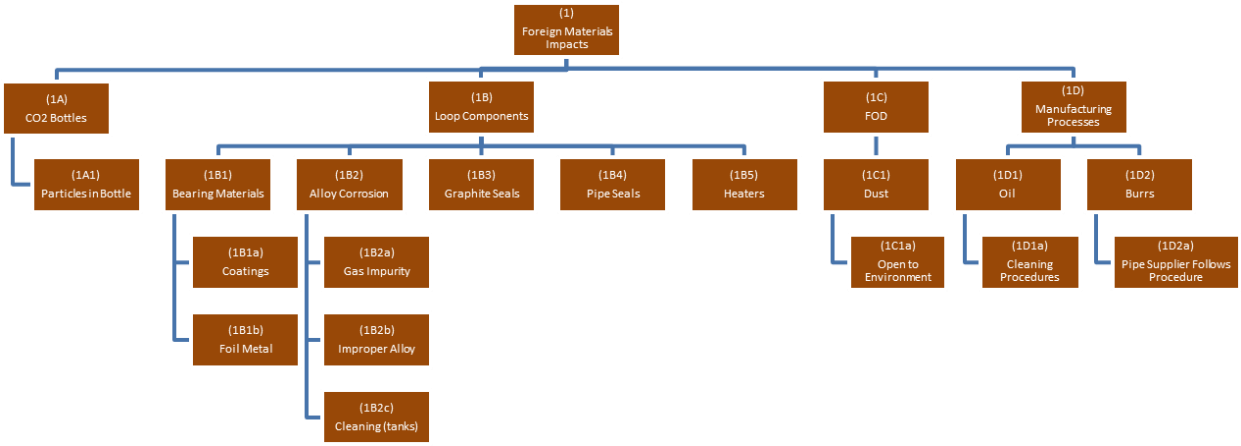

Figure 6: Turbine degradation RCA fault tree branch on foreign material impacts.

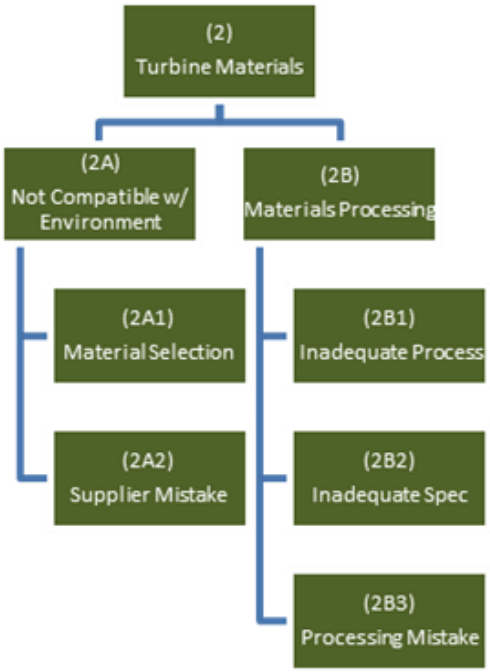

Figure 7: Turbine degradation RCA fault tree branch on turbine materials.

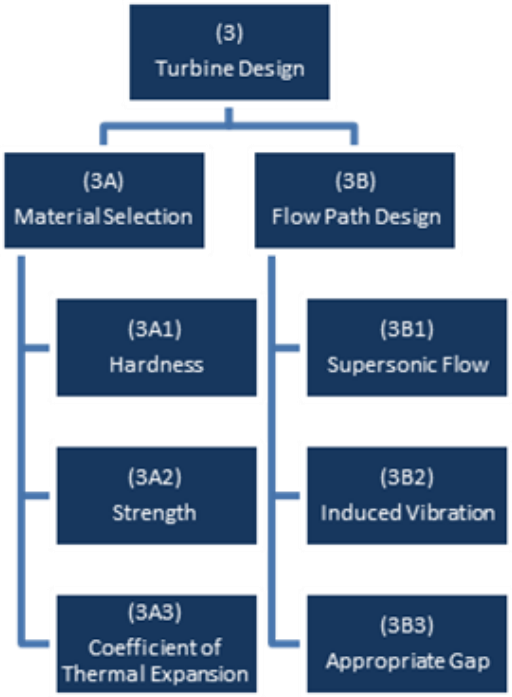

Figure 8: Turbine degradation RCA fault tree branch on turbine design.

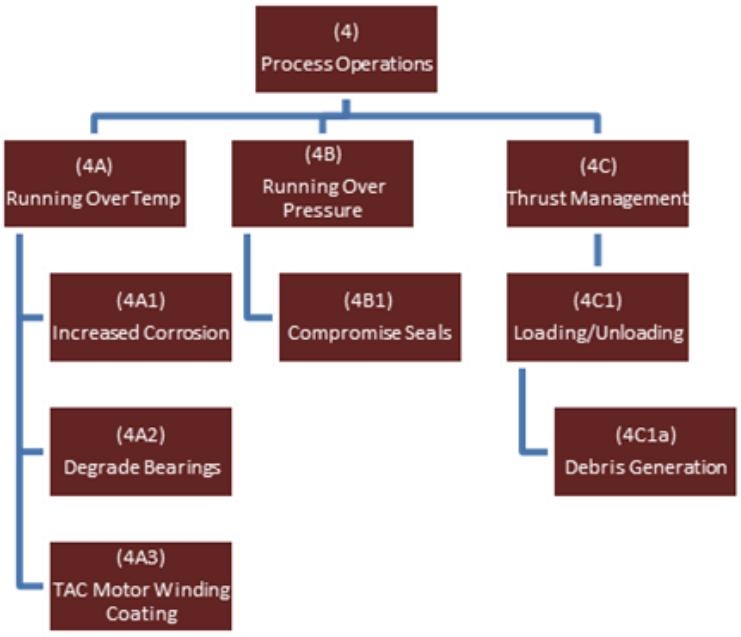

Figure 9: Turbine degradation RCA fault tree branch on process operations.

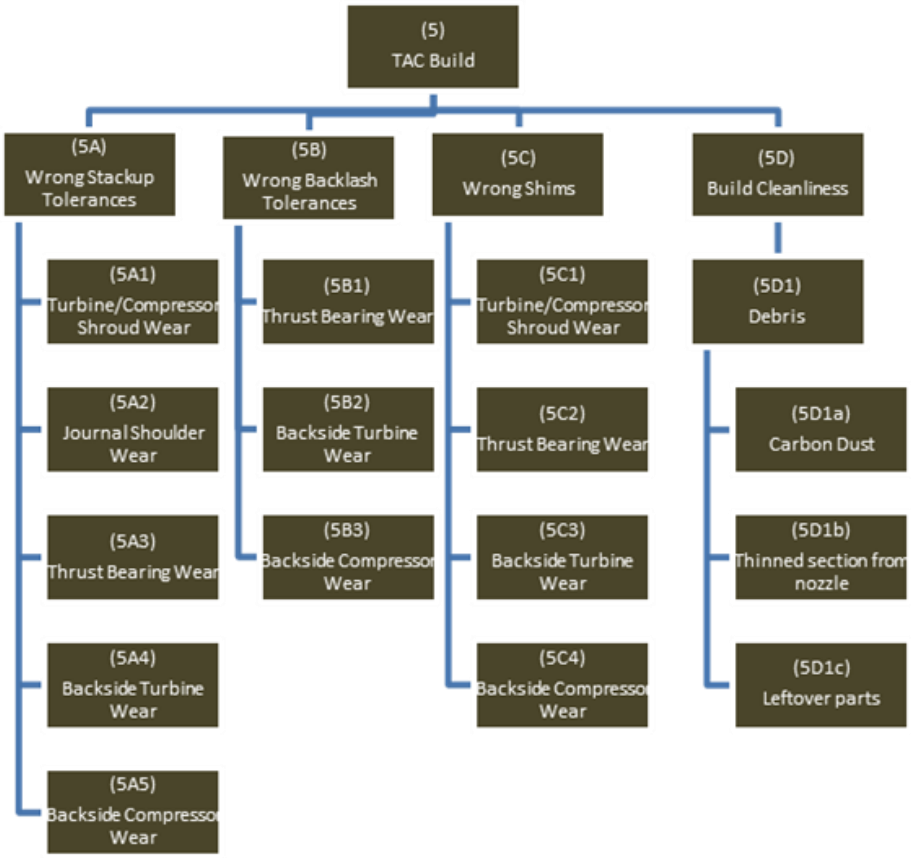

Figure 10: Turbine degradation RCA fault tree branch on TAC Build.

Table 1: TPR for identifying root cause of turbine degradation.

Item #	Main Category	Sub Category	Potential Root Cause	Rationale	Plan for Proving/Disproving	Key Elements	Owners
1	Foreign Materials Impacts	CO2 Bottles	Particles in Bottle	gas siphoned from bottom of bottle, may pull in particles	Can add filter to exit line from bottles, but concerned over pressure drop. Other concern is that not all bottles may have particles. Solution is an offline experiment where multiple gas bottles (~ 6) are blown down through a filter that is installed. Post-blowdown the filter is checked for particles. Need to find a filter for this.	(1) Offline Experiment using Filter	Fleming, Sharpe, Walker
2	Foreign Materials Impacts	Loop Components	Expansion Tank Corrosion	tanks have not been cleaned since SNL	Two ideas were discussed. One is to take a tank off-line and to pig it out, checking for and detecting loose particles on the tank interior. The second option, and more preferable starting point, is to first do an offline experiment where a filter is installed at the exit from the expansion tanks. This experiment would be combined with the CO2 bottles experiments, where the expansion tanks would be filled and then evacuated into the filter that is installed. If particles are detected in the filter during this test, then one of the tanks would be taken out and pigged to check for particles.	(1) Boroscope Inspection. (2) Offline Experiment using Filter	Fleming, Sharpe, Walker
3	Foreign Materials Impacts	Loop Components	Heater Corrosion	never looked inside	Start with a boroscope inspection of the inside of steel shells around the heating elements. The goal here is to check for what appear to be loose particles inside of these shells on shell walls or heating elements themselves. If nothing is found here, then eliminate this as a possibility and move on to others. If corrosion appears evident, then do an offline experiment where a filter is installed at the exit of the heater section, and a slow flow of gas is passed in through the heaters to this filter.	(1) Boroscope Inspection. (2) Offline Experiment using Filter	Fleming, Sharpe, Walker
4	Foreign Materials Impacts	Loop Components	Burrs	we have found burrs	Use the boroscope to do a complete loop inspection for burrs. If there are no burrs identified, then eliminate as a cause since we still are seeing turbine degradation in the absence of burrs. If burrs are present, then we need to go in and smooth these out, and then see how this may influence turbine degradation on future test loop runs.	(1) Boroscope Inspection	Fleming, Sharpe, Walker
5	Turbine Materials		Supplier Mistake	Not sure about current processing of 718 parts, or if these can impact hardness of completed parts.	It seems that this may have already been adressed by the turbine vendor. Need to verify and understand their record keeping process.	No experimental work	Kruzenga, Walker
6	Turbine Materials		Inadequate Process	Understand turbine materials processing steps. Understand how materials hardness is affected by these.	This will be rolled into work with Concepts NRC --- They will look over our design and run thermal analyses to ensure that thermal growth is not an issue and that we have proper clearance with current materials and flow path design	No experimental work	Kruzenga, Walker
7	Turbine Design	Materials Selection	Coefficient of Thermal Expansion	seen this before just did analysis there are thermal growth issues	This will be rolled into work with Concepts NRC --- They will look over our design and run thermal analyses to ensure that thermal growth is not an issue and that we have proper clearance with current materials and flow path design	No experimental work	Fleming
8	Turbine Design	Flow Path Design	Appropriate Gap	very possible due to dissimiliar materials with thermal growth	Start with an inspection of all bearing surfaces for wear. All particles generated during thrust issues would pass through to the hydropac. So, the second step is to inspect the hydro pac cylinder walls for wear/erosion. Use boroscope for this?	No experimental work (1) Visual bearing inspection (2) Boroscope inspection of hydropac cylinder walls	Fleming
9	Process Operation	Thrust Management	Loading/Unloading	we do have thrust problems			Fleming, Sharpe, Walker
10	TAC Build	Turbine/Compressor Shroud Wear	Wrong Stackup Tolerances	we have had this before when building	We are going to wait on these for now. We will move to these if we have completed items 1-9 without identification of the root cause for Turbine Degradation		
11	TAC Build	Turbine/Compressor Shroud Wear	Wrong Shims	we have seen this			

2.4. sCO_2 Loop Inspection (June 2016)

In an effort to investigate the possible root causes associated to foreign material impacts, USA Borescopes (Clarksville, TN) was hired to perform a full borescope inspection of the sCO_2 Brayton Cycle test loop. For three days in June 2016 they worked with our Sandia team to complete this invaluable inspection, using a variety of Borescopes to take photos and videos from within the loop. Meanwhile, samples of foreign materials were collected from within the loop. After completing the borescope inspection of an area, a modified vacuum was used to collect any debris that was present within that area.

Figure 11 shows a diagram of the test loop that includes locations where foreign material was identified and collected. Images were taken for 22 total samples of foreign material collected from the test loop using the SEM. Also, some chemical information for these particles was collected using EDS. Supplementing these analyses was a more in-depth chemical analysis for four of the powders, using x-ray diffraction (XRD).

Following these inspections, the main focus areas were the expansion (or inventory) tanks, high temperature recuperator (HT Recup), heaters, and sections of piping running between Motor/Gen B (TAC B) and both the heaters and HT Recup. These are areas where significant foreign material debris was identified, and it may be leading to turbine degradation during operation of the test loop.

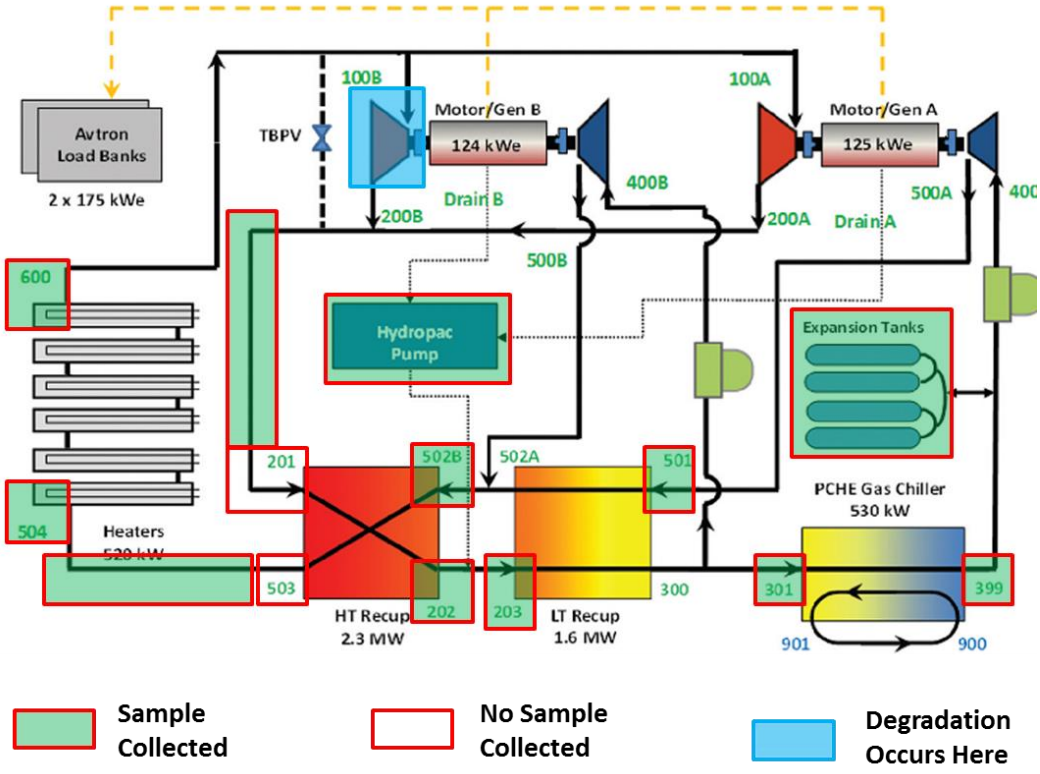

Figure 11: Diagram of the Sandia SCO2 test loop, including locations where foreign material were identified and collected.

Within the design of the test loop, gas flows into the expansion tanks from the Hydropac pump and flows out from the expansion tanks back into the test loop near the HT Recup inlet at 502A. Several images of the expansion tanks are shown in Figure 12. The tanks are made of carbon steel, and all twelve of them are connected in series, with gas entering one end of a tank and exiting through the other. Gas from the Hydropac pump flows into tank 1, and then continues through each tank until it exits tank 12, back to the loop.

The borescope inspection of the tank interiors revealed a significant quantity of foreign material. A few images of the debris are shown in Figure 13. Visually, it resembled a mixture of metal shavings, glass fibers (likely fiber glass insulation), and metal oxidation product that had spalled from the interior cylinder walls. Samples of foreign material were extracted from each of the tanks, providing for a full characterization of its constituents. An SEM image of this foreign material is shown in Figure 14. EDS of this material revealed that it had a predominantly Fe-O chemistry, indicating that the debris was likely a combination of carbon steel shavings (Fe) and oxidation product (Fe_2O_3).

Leading up to this inspection, it was hypothesized that these tanks contained metal oxidation product debris that was flowing into the loop and causing turbine degradation. This was thought to result from prior hydro-testing that was done in these tanks. Following the inspection, it was evident that this hypothesis may indeed be true, as foreign material in support of it was found within the tanks. However, for this hypothesis to be confirmed the presence of Fe_2O_3, without chromium, needed to be present in the main part of the sCO_2 system (to be discussed later).

Figure 12: Expansion (or inventory) tanks.

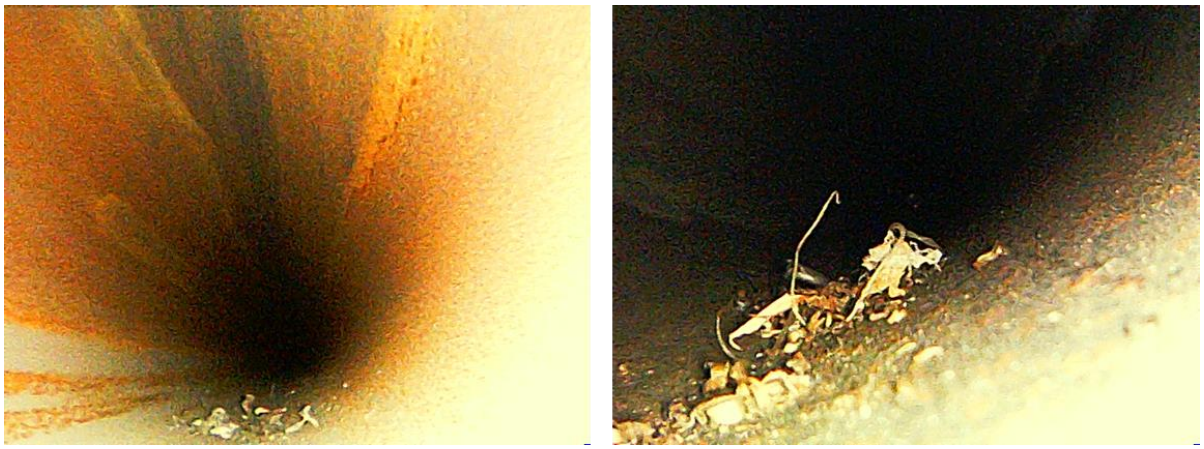

Figure 13: Figure 40. Images of debris within the expansion tanks, as captured by borescope.

Figure 14: SEM image of foreign material from the expansion tanks.

The HT Recup has four separate manifolds directing CO_2 flow across its channels. An image of the HT Recup is shown in Figure 15. After exiting the turbine, hot CO_2 enters the HT Recup at manifold 201, and exits at manifold 202. Flowing in the opposite direction, cool CO_2 enters at manifold 502B and exits at manifold 503. Each manifold was inspected using the borescope. Images of the fluid flow channels within each manifold are shown in Figure 16. Fluid flow channels at manifolds 201, 502B, and 503 appeared clean, and free from surface contamination or corrosion product. In the case of manifold 202, there was a surface film (contamination or corrosion product) covering the fluid flow channel surface. Foreign material was collected from within manifolds at 502B and 202, while none was found in the other two manifolds. It is unclear why just the one surface was contaminated while the others were clean, or why two of the manifolds contained debris while the others did not.

Figure 15: Figure 42. HT Recuperator showing the four manifolds.

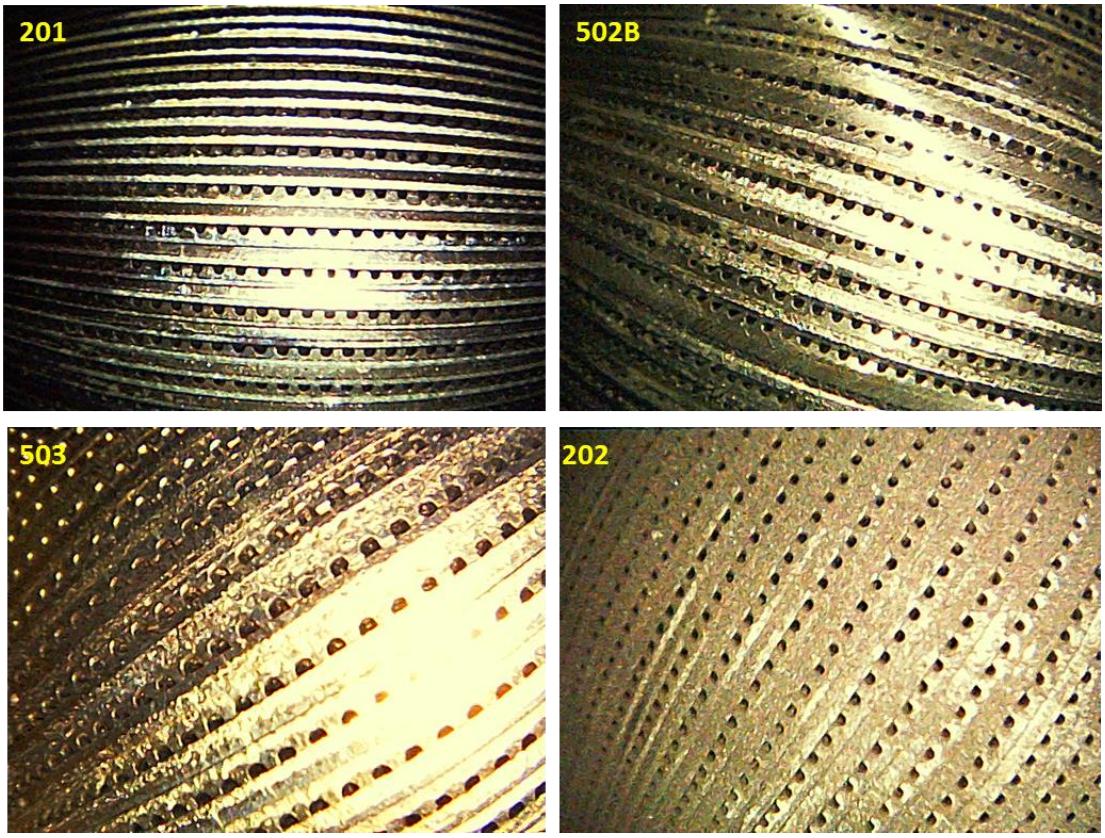

Figure 16: Fluid flow channel surfaces for the four manifolds of the HT Recup.

SEM images of the debris collected from the manifolds at 502B and 202 are shown in Figure 17. In both instance, there are predominantly particles which show up dark, along with fewer light particles. The darker particles appear to be stainless steel having a chemistry of primarily Fe-Cr-Ni. In some instances these particles have the appearance of metal shavings. The lighter particles appear to be oxides having a chemistry that contains Si-Al-O, among others.

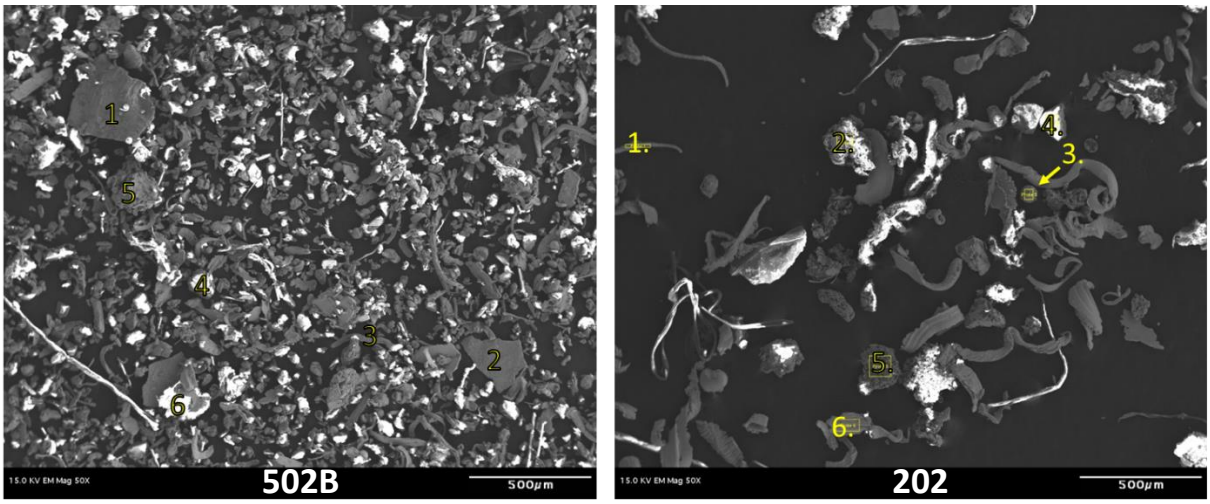

1. Fe, Cr, Ni, Mo, Cu, Si
2. Fe, Cr, Mn
3. Fe, Cr, Ni, Mo
4. Si, O, Cl
5. Fe, Cr, Ni, Al, O
6. Fe, Cr, Ni, Si, O, Cl

1. Fe, Cr, Ni, Si, O
2. Si, Ti, O, Fe
3. Fe, Cr, Ni, O
4. Si, O, Al, Na, Ca, Cl, Mo
5. Si, O, Al, Ca, Cl, K, Fe
6. Fe, Cr, Ni, Al

Figure 17: SEM images and EDS chemistry of debris collected from the HT Recup at manifolds 502B (left) and 202 (right).

The primary gas heaters are comprised of steel tanks connected in series; within each tank is an alloy sheathed heating elements. Borescope inspections were completed at both the inlet and outlet to these heaters, but could not be completed through the entire heated pathway without significant teardown of the loop. The gas heaters were opened in January 2017 for clean-up and inspection, where a more through discussion/analysis is provided in the next section.

Referring back to the loop diagram in Figure 11, the inlet is shown as 504, while the outlet from the heater is shown as 600. Images of these two locations are shown in Figure 18. Interior photos of each are shown in Figure 19. The areas of the heaters that could be inspected using the borescope appeared to have some oxidation, but overall were relatively clean. The exception to this was an area near the entrance to the heaters that had a rather large pile of debris. An image of this debris is shown in Figure 20. A sample was extracted from the heater for analysis. An SEM image of this material is shown in Figure 21. Similarly to the material from the HT Recup, the material appears to be predominantly stainless steel shavings along with a few oxide particles, an indication that carbon steel inventory tanks may not be the source of particulate contamination.

Figure 18: Inlet (A) and outlet (B) for the SCO2 test loop heaters.

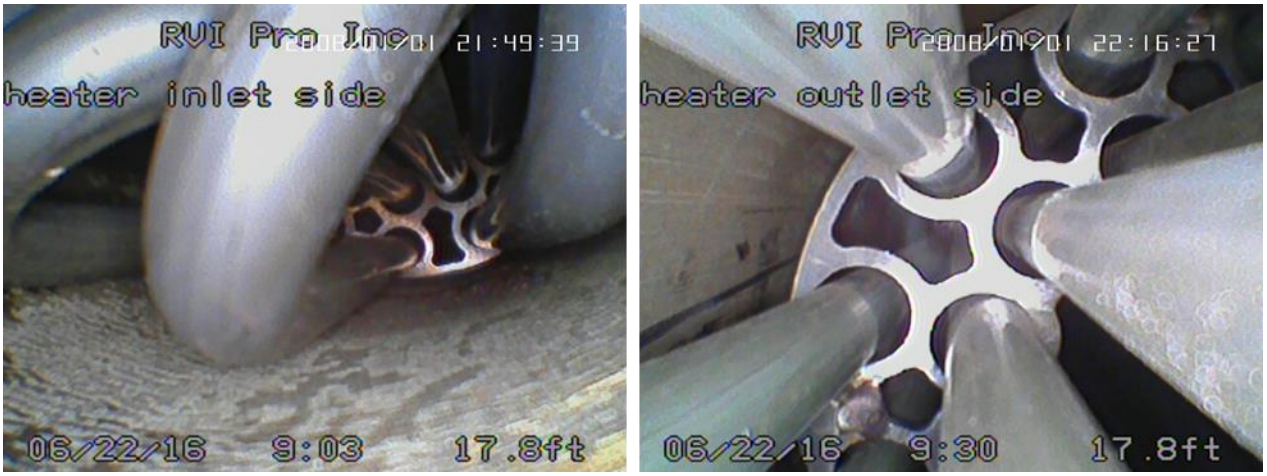

Figure 19: Interior photos of the inlet and outlet areas of the heaters.

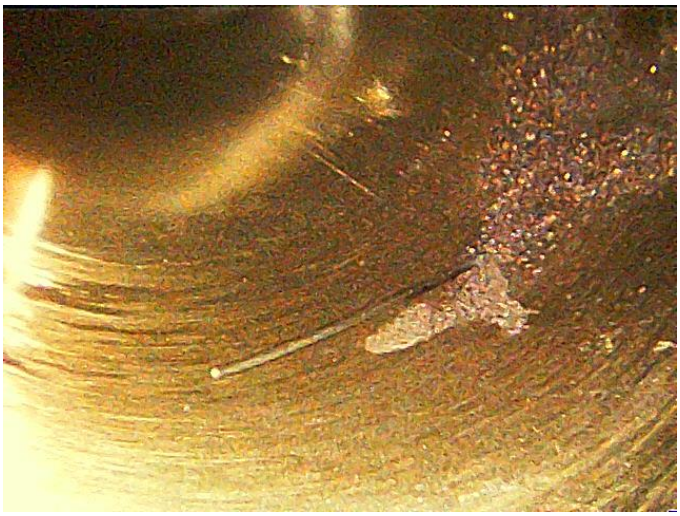

Figure 20: Image of foreign material debris within the heater inlet at 504.

1. Al, O, Na, Si
2. Fe, Cr, Ni
3. Fe, Cr, Ni
4. Fe, Cr, Ni

Figure 21: SEM image and EDS chemistry of debris collected from the heater inlet.

Although the entire length of pipe for the test loop system was inspected using the borescope, the areas of most interest associated to turbine degradation were sections of pipe running between Motor/Gen B and both the heaters and HT Recup. An image of the pipe interior for the section between the HT Recup and the heater inlet is shown in Figure 22. Foreign material in these sections of pipe was not visually evident using the borescope, but a small quantity was collected using the vacuum method. An SEM image of this material is shown in Figure 23. As was the case with both the HT Recup and the heater inlet, the material is predominantly stainless steel having a chemistry of Fe, Cr, and Ni. Again, oxides of Al and Si were also present.

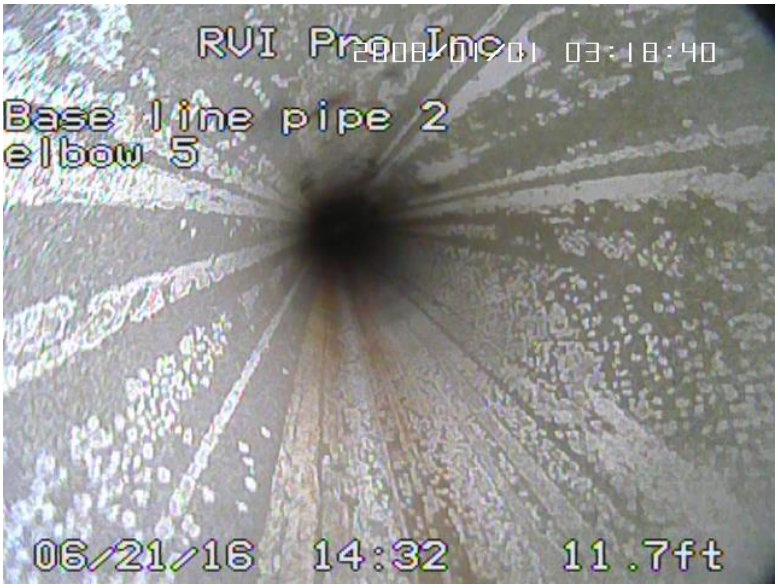

Figure 22: Image inside pipe section between HT Recup (503) and heater inlet (504).

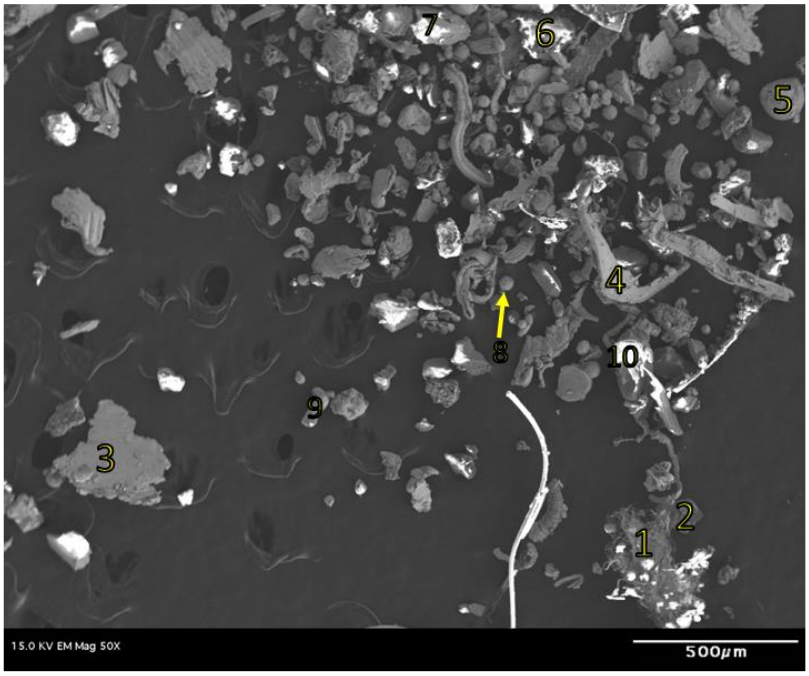

1. O, Fe, Si, Cu, Cr, Cl
2. Si, O, Al, Mg, Fe, K
3. Fe, Cr, Ni
4. Fe, Cr, Ni
5. Fe, Cr, Ni, O
6. Si, O
7. Si, O
8. Fe, Cr, Ni
9. Fe, Cr, Ni, Cu
10. Al, O

Figure 23: SEM image and EDS chemistry of debris collected from the pipe section between HT Recup (503) and heater inlet (504).

Having a more complete understanding of the foreign material chemistry is useful in comparing the material chemistry between the various locations. As such, four materials were selected for XRD analysis. These included material from the HT Recup at 502B and 202, the heater inlet at 504, and the expansion tanks. Photos of these four materials are shown in Figure 24. Visually, the material from the expansion tanks appeared different than the other three, while the others appeared more similar to each other. The expansion tank material had a reddish-orange color, likely indicating the presence of hematite (Fe_2O_3), which forms during oxidation of carbon steel in CO_2 but not of stainless steel. For stainless steel, oxidation in CO_2 typically results in the formation of both Cr_2O_3 and Fe_3O_4. Neither of these has the reddish-orange color of hematite.

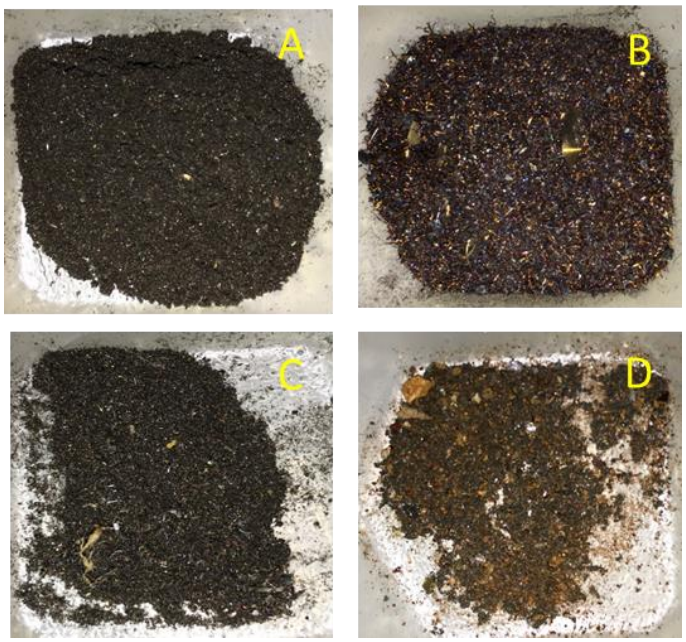

Figure 24: Foreign material collected for chemical analysis from the HT Recup at 502B (A) and 202 (C), heater inlet at 504 (B), and the expansion tanks (D).

The XRD patterns collected for these four materials are shown in Figure 25. Here, peak indexing indicates a matching chemistry for all of the materials except for that of the expansion tank. The materials from the HT Recup and heater inlet indicate the presence of predominantly stainless steel along with oxides of aluminum and silicon. The chemistry for the material in the expansion tanks is quite different, with no noticeable correlated peaks between them. This provides a strong indication that the material within the expansion tanks is not flowing out into the test loop. The converse, material flowing from the loop into the expansion tanks, is also not occurring. This information eliminates the hypothesis of foreign material from the expansion tanks being the cause of turbine degradation, as it does not appear that this material ever leaves the tanks.

Particle size analysis was performed on samples from a select number of locations. This was done to identify any particle size trends that may exist for various locations. Analysis was performed at Particle Technology Lab (PTL) in Illinois using image analysis techniques.

Image Analysis was performed using a Malvern® Morphologi G3S image analyzer. This is an automated microscope that uses a series of varying magnifications, a motorized stage, and a 5-megapixel camera to capture images of particles in order to determine size and shape. Range on this instrument is from 0.56µm to 1000µm. This method captures the circular equivalent weighted on either a number-basis or volume-basis and, additionally, information on aspect ratio $\left(\frac{width}{length}\right)$ and circularity $\left(\frac{2\sqrt{\pi * area}}{perimeter}\right)$ are also reported.

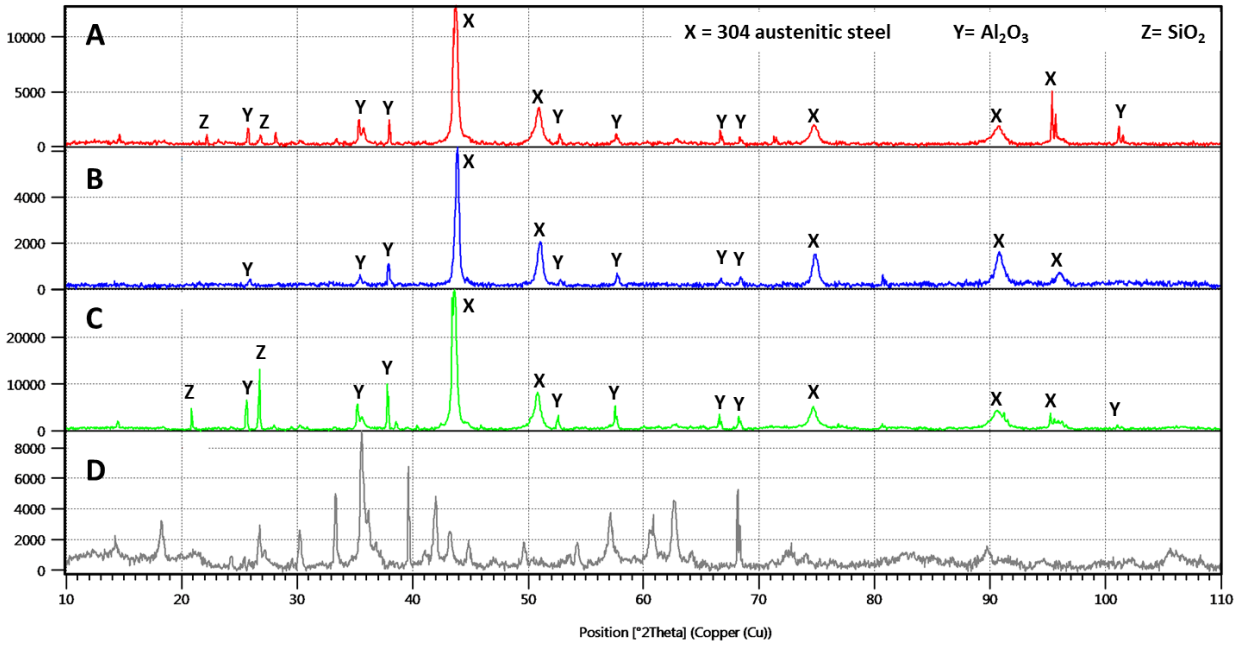

Figure 25: XRD patterns for foreign material from the HT Recup at 502B (A) and 202 (C), heater inlet at 504 (B), and the expansion tanks (D).

Two locations were investigated; the inlet to the primary gas heater (location 504) and the inlet to the HT recup (location 502B). Based on the results there are clear trends in particle size vs. location. Image analysis results are provided for size distribution, aspect ratio (AR), and circularity with a snapshot of results in Table 2 and Figure 26.

Table 2: Image analysis results for circular equivalent diameter, aspect ratio, and circularity

Location		Ave Diameter [µm]	Standard Deviation (STDV) Diameter [µm]	Ave AR	STDV AR	Ave Cir	STDV Cir
502B	High Temp Recuperator	22.1	20.6	0.67	0.18	0.87	0.11
504	Heater Inlet	11.1	23.6	0.73	0.17	0.90	0.11
AR for a circle/square is 1.0, 2:1 rectangle is 0.5 Circularity of a square is 0.886							

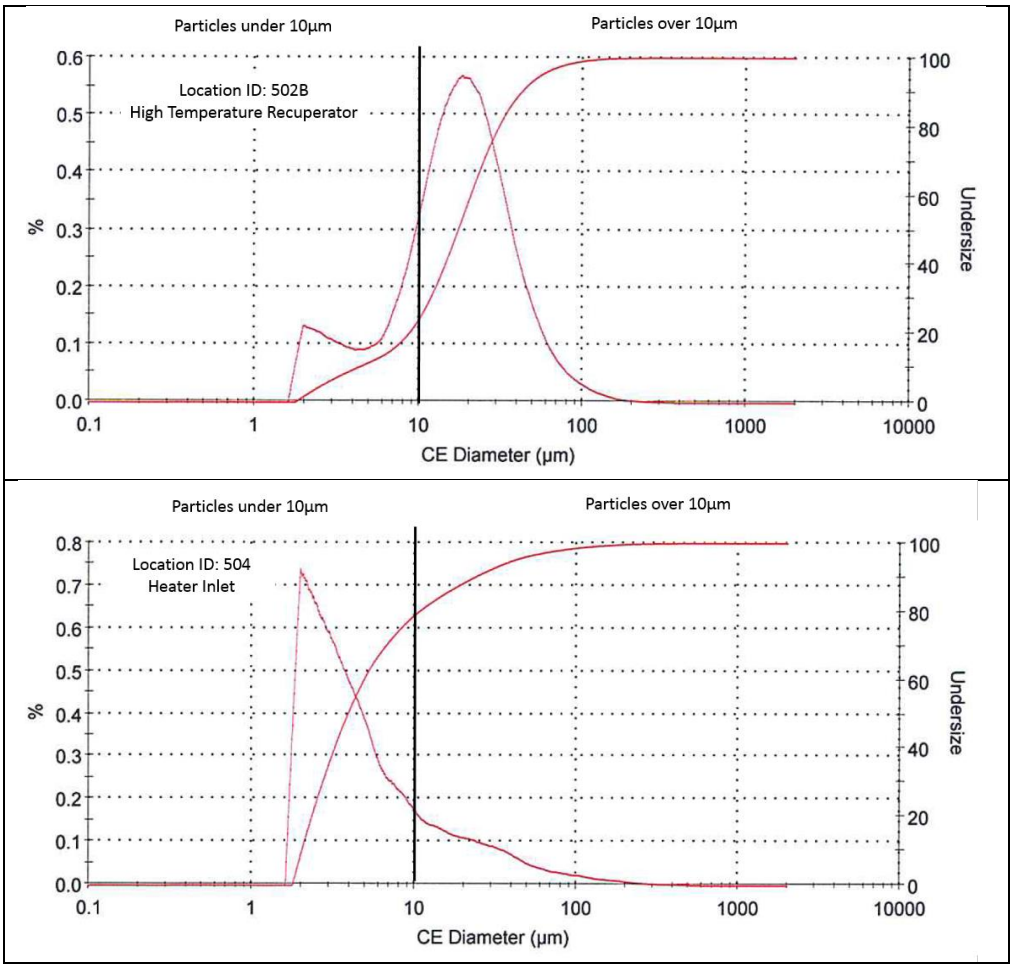

Figure 26: Particle distribution for both locations investigated. Line indicates minimum available 10µm filter size available.

2.5. Primary Gas Heater Particulate Analysis (January 2017)

In January 2017 the primary gas heater (refer to Figure 11) was opened up and cleaned between locations 504 and 600.

Chemical forensic analysis (performed by EAG Laboratories) of samples from each location indicated a mixture of organic and metallic elements. Based on the elemental analysis the metal detected was likely 316, based on the high molybdenum content (316L is the piping materials used in the Brayton system). Particle geometry analysis (performed by PTL) indicated that the particles found in this area were much smaller (see Table 3) than those analyzed previously. Particles found in the heater inlet during the inspection in early 2017 (Table 3) were roughly half the diameter of particles found in the summer of 2016 (Table 2).

Table 3: Particle size distribution in the primary gas heater.

Location		Ave Diameter [µm]	Standard Deviation (STDV) Diameter [µm]	Ave AR	STDV AR	Ave Cir	STDV Cir
504	Heater Inlet	5.4	15.1	0.74	0.14	0.93	0.07
600		5.3	18.9	0.75	0.14	0.94	0.07
AR for a circle/square is 1.0, 2:1 rectangle is 0.5 Circularity of a square is 0.886							

2.6. RCA Conclusions and Corrective Actions

The diameter of the collected particles found in the heater inlet were half the size of particles found in the high temperature recuperator, while AR and circularity were nearly identical at both locations.

Several questions arose from this data:

1. Is there any significance that chemically particles are metal (vs. an oxide)? (As reported in FY16)
2. Does the size difference provide any evidence as to what is occurring in the system?

An underlying assumption is that matter collected from the system are of the same origin. **Question 1 provides critical information:** *these particles were not fully oxidized, indicating that a corrosion induced spallation event did not cause damage in this situation.* Corrosion is not the source of the collected material. Inadequate cleaning from a loop modification is one possibility (i.e. drilling holes in pipe). Debris gathered from this entire exercise is on the order of 10g, so this little amount of material could have been overlooked by mistake.

If a loop modification resulted in debris then this leads to addressing **Question 2:** *larger particles would be closest to the contamination source.* Different particle sizes would have a varying propensity to being swept throughout the loop. Larger particles would be more difficult to move around, while the smaller and lighter particles should be more readily carried along in the sCO_2 flow.

While this explanation is reasonable and generally confirmed by data, one key observation has not been addressed: **why has the nozzles/turbine, made of high strength alloy 718, suffered damaged during operation while the compressor, made of the aluminum alloy 6061, has suffered no damage?** Two thoughts are offered in view of this observation.

First, the turbine is the highest velocity portion of the system so, due to the higher forces present, the force imparted by particle impingement will be most severe in the turbine region. Particles will have the highest kinetic energy in the turbine, where the influence of velocity is squared; i.e. $0.5mv^2$; m is particle mass and v is particle velocity.

Second, the heaters and heat exchangers all behave as particle traps. This was verified by finding most particles in heat exchangers. Flow transitions, from pipe to heat exchanger header, resulted in an abrupt change in the average flow velocity that functioned as an inertial filter.

2.6.1. Corrective Actions

Based on the analysis and discussion above the following two items are suggested for immediate implementation with a third suggestion as a best practice:

1. A particle filter, capable of going to at least 10µm, should be placed in the RCBC immediately. This will test the proposed hypothesis and also to protect the turbomachinery. This has already been implemented as of this document (see the next section for more description).

2. Implement a 10 µm (or smaller) filter between the CO_2 bottles used to fill the RCBC and RCBC itself. Concerns arose that not all contamination was from loop modifications, but possibly from contaminated bottles. A simple and practical process improvement that would both rule out the possibility of bottle debris and should help to avoid any dust that could enter the RCBC during fill.

3. Place a 10 µm (or smaller) filter between the inventory tanks and the RCBC. While no particulate matter seems to enter the RCBC this is an inexpensive solution to avoid the possibility of contamination.

2.7. Summary and Next Steps

At the outset of this RCA process, the leading hypothesis for turbine degradation was that foreign material (spalled corrosion product) from inside the expansion tanks was the cause. Although there was certainly a significant quantity of foreign materials found within these tanks, chemical information obtained from the foreign materials appears to disprove this hypothesis. The crossover of material from these tanks to the test loop, that one would expect to see if this was the cause of degradation, was not found to occur. The foreign material within the loop was found to be stainless steel along with some oxides of silicon and aluminum. The material within the expansion tanks was quite different, having a chemistry of primarily iron and oxygen.

Based upon analysis performed above, the leading hypothesis is that small stainless steel particles are still present in the system – likely from the piping, which is 316L. Mitigation is the inclusion of a filter to remove particles, as the reason for why particles are present is still unknown.

2.7.1. sCO_2 In-line Filter

As part of the RCA process, as suggested in the previous section, an sCO_2 filter was purchased from Norman Filter Company, LLC. (Bridgeview IL). Prior to purchasing this filter, calculations

were performed to determine maximum pressure drop across a 10 µm filter. Data was well represented using a quadratic.

The pressure loss for the filter can be calculated as the sum of the pressure resistance due to the filtering element (i.e. mesh screens) and the resistance through the pipe:

$$\Delta P = \sum \Delta P_{element} + \Delta P_{pipe}$$

ΔP_{pipe} is calculated based upon flow regime (i.e. turbulent vs. laminar) for the given pipe. Figure 27 indicates that the pressure through the pipe tends to dominate the overall pressure drop as larger mesh sizes are used (labelled on the plot). $\Delta P_{element}$ in the plot was determined from a NASA study (NASA-CR-140386) where empirical fits are provided for the various filter architectures. For the 325x2300 mesh the following is suggested:

$$\Delta P_{element}[psi] = aQ^2 + bQ$$
$$Q: \left[\frac{GPM}{EA}\right]; EA\ is\ element\ area\ (in^2)$$
$$a = 0.19\frac{\rho_{fluid}}{\rho_{H2O}};\ \rho\left[\frac{lbm}{ft^3}\right];\ (\rho_{H2O} = 62\frac{lbm}{ft^3})$$
$$b = 1.45\mu_{fluid};\ \mu_{fluid}[cP]$$

Using this set of equation will provide an estimate of the flow rates expected through the filter. An example is as follows using Figure 27:

At a flow rate of 600GPM, the pressure drop <u>over the mesh element only</u> is 2.1psi. At 600GPM the pipe pressure drop is ~1psi, so therefore the total pressure drop of the 325x2300 mesh is ~3psi. This correlates well with the values provided on the graph below and should be used to calculate pressure drop in the RCBC.

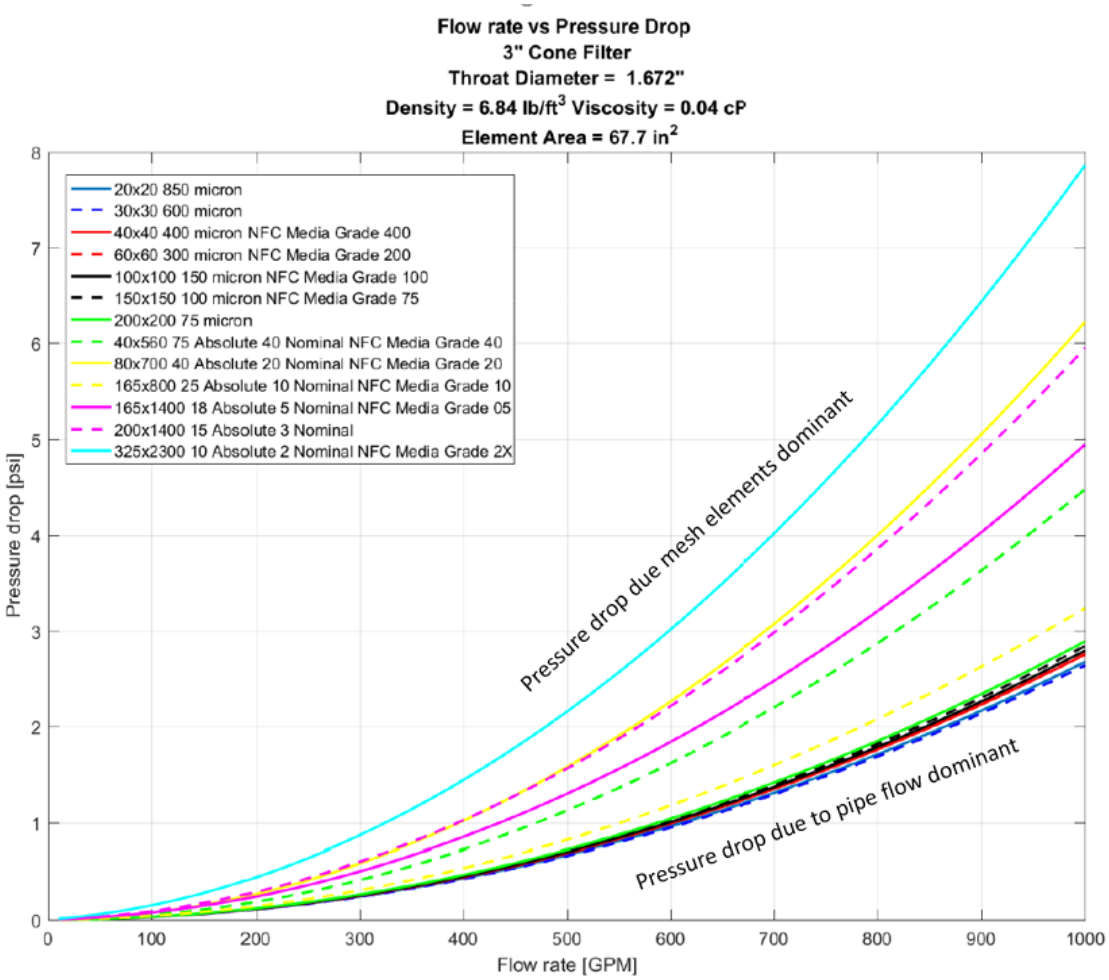

Figure 27: Pressure drop curve from Norman Filters

Figure 28 shows both the drawing and some photos of the filter, which was fabricated from 316L with Norman's minimum filter screen of 10µm. The filter was bolted to a Graylok ring to provide flexibility in moving among various locations within the RCBC. Detailed drawing supplied from Norman Filters is located in Appendix I: Materials Engineering Support Update, Quarter 2, Fiscal Year 2017 along with other design information.

Filter Test Plan:

Test 1: Install the filter at the split T going to each of the Turbine-Alternator-Compressors (TACs). This is located nominally at 100B per the schematic in Figure 1. By placing this directly upstream of the turbines, it should catch any particles that would normally travel from the loop into the turbine, potentially causing the degradation of these components. Post-test the filter will be removed and inspected for debris, i.e. pictures, record weight, and sent out for analysis.

The filter was in this location at 100B for one test of the CBC. It is desirable to maintain the filter in this location through multiple runs, but thus far there haven't been additional runs. Once the

filter has achieved multiple runs in this location, then the filter will be removed and inspected for debris.

Subsequent tests will involve moving the filter further upstream of the TACs to determine if particles are being generated in various locations of the CBC. Several examples of possible follow-on tests are below:

Test 2: Move the filter to the heater outlet, corresponds to 600 on the schematic
Test 3: Move the filter to the heater inlet, corresponds to 504 on the schematic
Test 4: Move the filter to the HT Recuperator outlet, corresponds to 503 on the schematic
Test 5: Move the filter to the HT Recuperator inlet, corresponds to 502B on the schematic

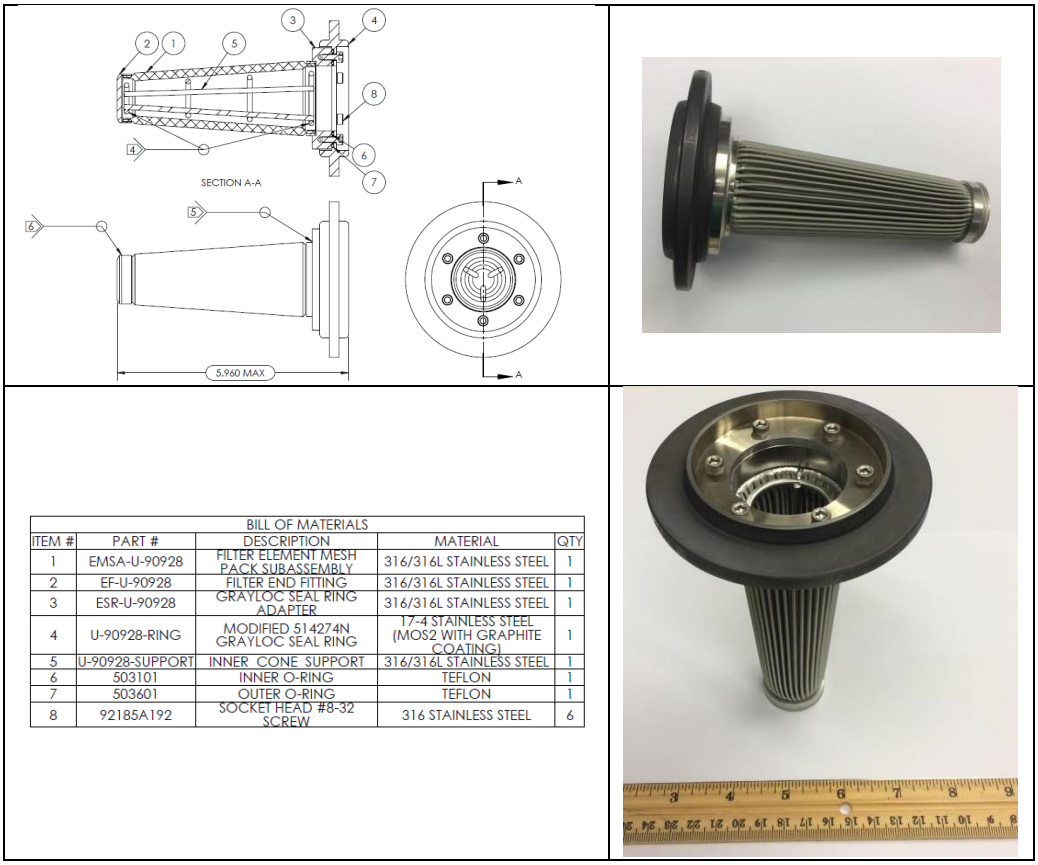

BILL OF MATERIALS

ITEM #	PART #	DESCRIPTION	MATERIAL	QTY
1	EMSA-U-90928	FILTER ELEMENT MESH PACK SUBASSEMBLY	316/316L STAINLESS STEEL	1
2	EF-U-90928	FILTER END FITTING	316/316L STAINLESS STEEL	1
3	ESR-U-90928	GRAYLOC SEAL RING ADAPTER	316/316L STAINLESS STEEL	1
4	U-90928-RING	MODIFIED 514274N GRAYLOC SEAL RING	17-4 STAINLESS STEEL (MOS2 WITH GRAPHITE COATING)	1
5	U-90928-SUPPORT	INNER CONE SUPPORT	316/316L STAINLESS STEEL	1
6	503101	INNER O-RING	TEFLON	1
7	503601	OUTER O-RING	TEFLON	1
8	92185A192	SOCKET HEAD #8-32 SCREW	316 STAINLESS STEEL	6

Figure 28: Design dimensions (in inches) and materials used for filter.

3. Real Time Health Monitoring

One of the areas identified for further research is real time equipment health monitoring. Health monitoring is a wide ranging topic and, in this context, the objective is to outline several of the various techniques that could be developed and eventually deployed in an RCBC. The two main monitoring areas discussed are corrosion monitoring and erosion monitoring as they pertain to needs within the RCBC.

3.1. Corrosion Monitoring

Corrosion monitoring, with real time feedback, was suggested as an additional metric to leverage during plant operation. Minimizing material corrosion during plant operation could greatly increase lifetime and improve overall performance, where the author gave the following example:

Perhaps the best parallel to the use of a sensitive real-time corrosion indication is to the experience of driving a car with a real-time indication of fuel consumption. Any person who has driven such a vehicle has surely been appalled by the drastic decrease in the indicated fuel consumption rate as soon as they press the accelerator. At the same time, lifting the foot from the accelerator when the vehicle is slowing down immediately produces a similarly amazing improvement in the consumption rate. Practically, the driver does not expect either indication to be particularly accurate. However, on checking the actual fuel consumption the next time the tank is refilled, there is no doubt that if the driver has tried to avoid harsh use of the accelerator the fuel consumption will be reasonable, whereas if he has been clumsy with the accelerator the evidence is clearly reflected by the speed that money disappears from his wallet. [3]

In this paper the author introduces conventional techniques and advanced techniques. Conventional techniques have been used in the oil industry since the late 1950s, are well understood and are readily available as commercial off the shelf. Electrical resistance (ER) is one of these foundational techniques and will be discussed in the next section. Electrochemical noise is another promising technique for sCO2 monitoring and is also briefly discussed.

3.1.1. Electrical Resistance Experiments

ER is a simple, robust technique that measures resistance across a metallic element. As the element increases in resistance due to corrosion this is correlated to a loss in the element thickness. This can be represented by the following equation:

$$R_{probe} = \rho \frac{L}{A}$$

Where ρ is volume resistivity, L is probe length, and A is probe cross sectional area. Probe area consists of width and thickness, therefore as the area decreases R_{probe} increases.

Probe and data acquisition were purchased from Metal Samples® shown in Figure 29. The probe was made custom for the temperature range in question and part of this test series has been to assess the robustness of the probe element. This probe consists of two resistor elements (Figure 30): the probe element, exposed to environment, and reference, which is hermetically sealed. Relative ratio of resistances account in internal temperature adjustment, thus the returned value indicates true metal loss.

Figure 29: Photo of 316L ER device with heat shield removed. Reference element internal to the device.

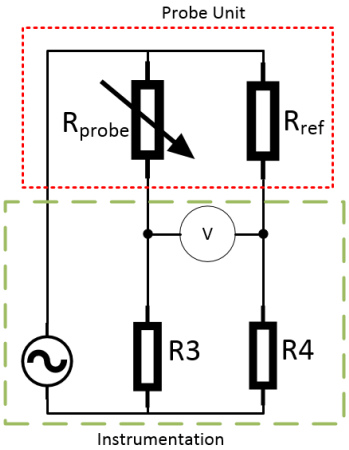

Figure 30: Schematic representation of ER device.

Figure 31 is a photograph of the corrosion probe installed in a quartz tube furnace. Shake down tests were performed in this arrangement at various temperatures and at isothermal conditions (650°C) in Argon and CO2 over the course of 1.5 months.

Thermal ramps and holds were performed (Figure 32) and the relative response of the probe (red symbols) indicate that as temperature increased so did the corrosion rate. Each isothermal hold lasted 24 hours. Initial values on these tests were not reported as values were high due to the initial oxidation of the probe and we felt they were not representative of the actual behavior.

An isothermal experiment, Figure 33, indicated a clear change in corrosion rate when gas was changed from Argon (minimally corrosive) to CO2. Argon was the cover gas for 20 days, while CO2 was the cover gas for only 14 days. The resistance response was linear during the CO2 exposure, and exhibited more severe corrosion (as expected) vs. Argon. More testing is needed, but qualitatively the probe is performing as expected at representative operating temperatures.

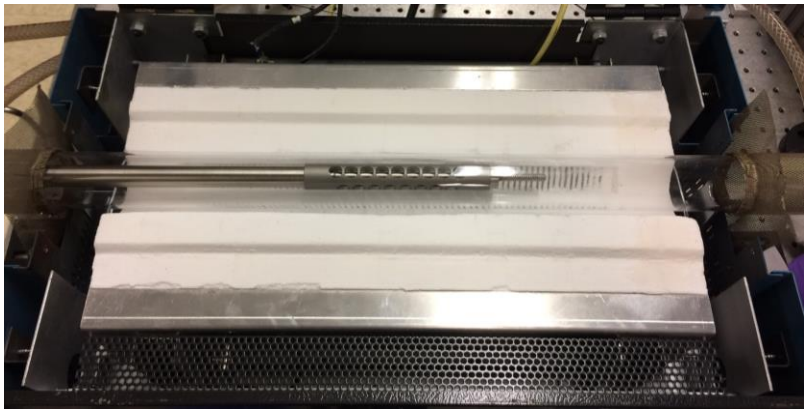

Figure 31: Probe, with heat shield, installed in quartz tube furnace

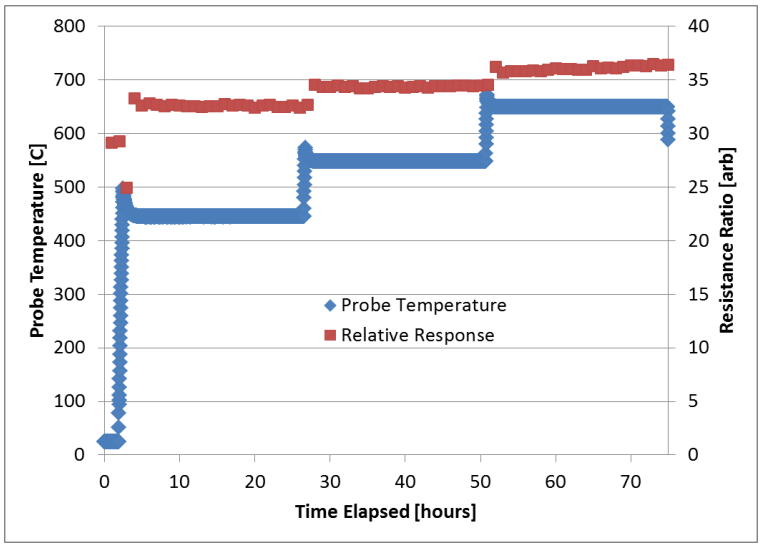

Figure 32: Thermal ramp and holds at three temperatures (CO2 cover gas)

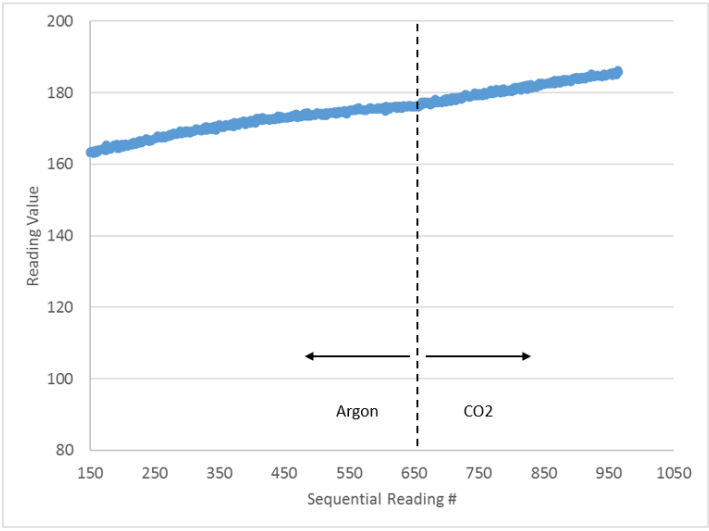

Figure 33: Inflection change indicates change in corrosion rate. ~15% increase in slope when CO2 was introduced (isothermal 650°C)

3.1.2. Electrochemical Noise

Electrochemical noise is typically considered an advanced corrosion monitoring technique. This technique uses electrodes, all made of the same material, where the current between electrodes (akin to a working and counter electrode) is measured and the potential is also measured (akin to a working and reference electrode)[4]. Collected data reflects natural fluctuations present in the system of question, as the signals are analyzed for standard deviations of both the current and potential noise. Potential noise divided by current noise is correlated to the polarization resistance through the Stearn-Geary relationship.

Advantages of this method are that it is a well suited for low conductivity fluids, specific to sCO_2, it is capable of measuring the real time corrosion rate, and has some ability to distinguish between various corrosion methods (i.e. pitting, uniform corrosion, stress corrosion, etc.). Disadvantages are lack of commercially available off the shelf systems, lack of experience in sCO2 systems with this technique, and relative complexity of the method.

3.2. Erosion Monitoring

Erosion monitoring is less common, but more often accomplished by witness coupon testing under controlled conditions. This is less helpful with regards to observing real-time material degradation, especially in the turbine section of the RCBC.

Upon a survey of existing technology, no solutions currently exist. Only one supplier was identified, and they had limited products that were able to achieve 450C/1500psi. Emerson Process Management (Roxar product line) has a product that is used to detect metal loss by detecting changes in the relative electric field within their device (see Figure 34) – this detects material loss in general, but does not provide information on mechanism.

Techniques able to achieve higher operating temperatures and pressures, relevant to sCO2 systems, would need to be pursued as a research and development project. The best path forward would be partnering with an industry entity and co-developing a product for high temperature/pressure applications.

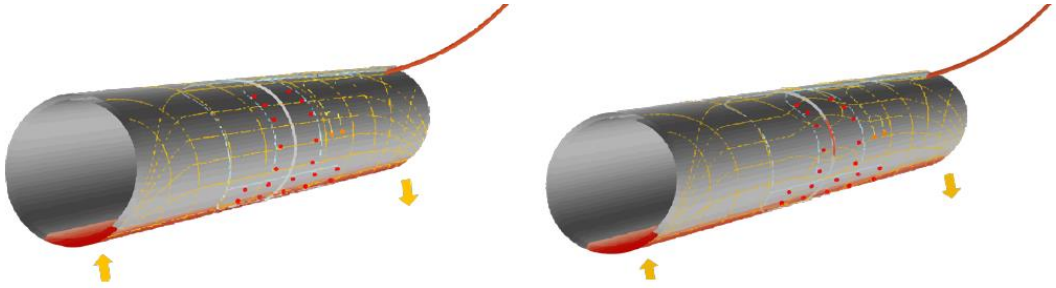

Priniciple of Field Signature measurements: An electric field is set up in an area of the pipe, and measured between pairs of sensing pins. Field pattern is changed if there is metal loss in the pipe, like a crack as shown left.

Figure 34: Field Signature Method (Roxar product data)

4. Conclusions

A root cause analysis has been performed on the RCBC. The major outcome is that the majority of particles found throughout the loop are stainless steel, likely alloy 316 based upon the elemental composition. Deployment of a filter scheme is underway to both protect the turbomachinery and also for purposes of determining the specific cause for the particulate. This will become clear as the filter is periodically removed and inspected for debris.

Shake down tests of electric resistance (ER) as a potential in-situ corrosion monitoring scheme shows promise in high temperature systems. A modified instrument was purchased and held at 650°C for more than 1.5 months to date without any issue. Quantitative measurements of this instrument will be benchmarked against witness samples in the future, but all qualitative trends to date are as to be expected. ER is a robust method for corrosion monitoring, but very slow at responding and can take several weeks under conditions to see obvious changes in behavior. Electrochemcial noise was identified as an advanced technique that should be pursued for the ability to identify transients that would lead to poor material performance.

No solutions currently exist for erosion monitoring instrumentation at the temperatures of interest. Further research and partnership development is required in this area. Until an adequate pathway is identified the recommendation of utilizing filtration to protect turbomachinery is suggested.

REFERENCES

1. Walker, M., et al (2016). Progress in Overcoming Materials Challenges with S-CO2 RCBCs: Final Report, Sandia Report: SAND2016-9774.
2. Dennies, Daniel P, *How to Organize and Run a Failure Investigation*. ASM International, 2005. Print.
3. Cox, W.M., A Strategic Approach to Corrosion Monitoring and Corrosion Management. Procedia Engineering, 2014. 86: p. 567-575.
4. Metals Handbook Desk Edition, J.R. Davis, Editor. 2013, ASM International.
5. Kresse, G., Furthmüller, J., *Phys. Rev.* B, 1996, 54, 11169.
6. J. P. Perdew, J. A. Chevary, S. H. Vosko, K. A. Jackson, M. R. Pederson, D. J. Singh, C. Fiolhais, *Phys. Rev.* B, 1992, 46, 6671.
7. J. P. Perdew, K. Burke, M. Ernzerhof , *Phys. Rev. Lett.*, 1996, 77, 3865.
8. E. Kim, A. Mohrland, P. F. Weck, T. Pang, K. R. Czerwinski, D. Tománek, *Chem. Phys. Letters*, 2014, 613, 59.
9. S. Dudarev, G. Botton, S. Savrasov, C. Humphreys, A. Sutton, *Phys. Rev. B,1998,* 57, 1505.
10. P. E. Blöchl, *Phys. Rev.* B, 1994, 50, 17953.
11. G. Kresse, D. Joubert, *Phys. Rev.* B, 1999, 59, 1758.
12. E. R. Davidson, *Methods in Computational Molecular Physics*, G. H. F. Diercksen and S. Wilson, Eds., Vol. 113, NATO Advanced Study Institute, Series C, Plenum, New York, 1983, p. 95.
13. Methfessel, M., Paxton, A.T., *Phys. Rev.* B, 1989, 40, 3616.
14. Monkhorst, H.J., Pack, J.D., *Phys. Rev.* B, 1976, 13, 5188.

Appendix I: Materials Engineering Support Update, Quarter 2, Fiscal Year 2017

The purpose of this memo is an update of root cause analysis (RCA) that began during Fiscal Year 2016 along with further updates of on-going engineering support provided to the Closed Brayton Cycle (CBC) located in Albuquerque, New Mexico. Updates consist of three distinct sections: particle analysis from the RCA in 2016, high temperature and pressure filter included in the CBC, and *in-situ* sensor development for identifying real-time corrosion on the CBC.

Attached is the memo for archival purposes.

Memo_RCA_Q2.docx